

# On the receding contact between a two-layer inhomogeneous laminate and a half-plane

Zhixin Liu<sup>a</sup>, Jie Yan<sup>b</sup> and Changwen Mi<sup>\*</sup>

Jiangsu Key Laboratory of Engineering Mechanics, School of Civil Engineering, Southeast University, Nanjing, Jiangsu 210096, China

(Received September 27, 2017, Revised March 18, 2018, Accepted March 19, 2018)

**Abstract.** This paper considers the smooth receding contact problem between a homogeneous half-plane and a composite laminate composed of an inhomogeneously coated elastic layer. The inhomogeneity of the elastic modulus of the coating is approximated by an exponential function along the thickness dimension. The three-component structure is pressed together by either a concentrated force or uniform pressures applied at the top surface of the composite laminate. Both semianalytical and finite element analysis are performed to solve for the extent of contact and the contact pressure. In the semianalytical formulation, Fourier integral transformation of governing equations and boundary conditions leads to a singular integral equation of Cauchy-type, which can be numerically integrated by Gauss-Chebyshev quadrature to a desired degree of accuracy. In the finite element modeling, the functionally graded coating is divided into homogeneous sublayers and the shear modulus of each sublayer is assigned at its lower boundary following the predefined exponential variation. In postprocessing, the stresses of any node belonging to sublayer interfaces are averaged over its surrounding elements. The results obtained from the semianalytical analysis are successfully validated against literature results and those of the finite element modeling. Extensive parametric studies suggest the practicability of optimizing the receding contact peak stress and the extent of contact in multilayered structures by the introduction of functionally graded coatings.

**Keywords:** receding contact; functionally graded coating; singular integral equation; Gauss-Chebyshev quadrature; finite element analysis

## 1. Introduction

In addition to advancing and stationary contact problems, receding contact represents another class of contact problems in which the contact extent decreases from its initial unloaded area during the course of loading application (Johnson 1985). In contrast, the contact area of the first two kinds of contact problems either expands or stays as a constant with increasing external loads. Receding contact typically occurs in layered structures characterizing the separation of a layer from an associated substrate. Engineering examples include asphalt pavements, train tracks, pad bearings, ship decks, floor boards, bed mattresses, transitional and interference pin-rod fittings, and among others. Receding contact threatens the health and integrity of multilayered structures and therefore has received extensive attentions of engineers and scientists for longer than a century (Rončević *et al.* 2016). The classical mechanical model that simulates the receding contact phenomenon considers an infinite elastic layer pressed against a semiinfinite substrate by either a concentrated

force or uniformly distributed loads. Although not the earliest to tackle the problem, Keer *et al.* (1972) first obtained the accurate receding contact size and contact pressure, by the use of elasticity theory.

The classical receding contact model of the layer-substrate type was continuously extended over last a few decades to take more influential factors into account. These efforts include introducing a surface traction of different distributions (Keer and Chantaramungkorn 1972, Tsai *et al.* 1974, Parel and Hills 2016), a solid indenter (Civelek and Erdogan 1974), frictional effects (Çömez 2010), a homogeneously coated layer (Adibelli *et al.* 2013), two unbonded layers both of finite thickness (Yaylacı and Birinci 2013, Yaylacı *et al.* 2014), a substrate composed of two quarter-planes (Erdogan and Ratwani 1974), a completely rigid substrate (Gecit 1986), an elastic substrate of finite thickness (Çömez *et al.* 2004), just to name a few. Another remarkable extension of the classical receding contact model is the replacement of the homogeneous elastic layer with a functionally graded material (FGM) whose material properties are allowed to vary continuously along its transverse dimension (El-Borgi *et al.* 2006). The semianalytical results found in El-Borgi *et al.* (2006) suggest that a hard FGM layer can effectively help to reduce the peak contact pressure, whereas for a soft one the opposite is true.

Analogously, variations of the FGM-substrate system have also been extensively studied in the literature. For example, this fundamental model was shortly extended to

---

\*Corresponding author, Professor

E-mail: [mi@seu.edu.cn](mailto:mi@seu.edu.cn)

<sup>a</sup>M.Sc. Student

E-mail: [liuzxpirl@163.com](mailto:liuzxpirl@163.com)

<sup>b</sup>Ph.D. Student

E-mail: [yan\\_jie@foxmail.com](mailto:yan_jie@foxmail.com)

axisymmetric case by Rhimi *et al.* (2009). Two years later, Rhimi *et al.* (2011) revisited the problem by replacing surface traction loads with a spherical rigid indenter. Liu *et al.* further explored the same axisymmetric model by discretizing the FGM layer into several sublayers with linearly varied shear moduli. By such an approximate, FGM layers with arbitrarily graded material properties can be addressed. The frictional version of the fundamental model has also been recently solved (El-Borgi *et al.* 2014). In addition, Adiyaman *et al.* (2016) analyzed an FGM layer supported by two elastic quarter-planes. Substrates other than an elastic half-plane have also been considered. For example, Adiyaman *et al.* (2017) investigated the loss of contact between an FGM layer and a rigid substrate under the application of gravity and a tensile surface traction over a finite interval. Yan and Li (2015) and Çömez *et al.* (2016) considered a homogeneous and an FGM substrate both of finite thickness, respectively.

These studies are all concerned with the receding contact occurring in structures composed of two layers (including the substrate), in which the FGM strip functions as an independent structural element. Nonetheless, in engineering practice FGMs are typically employed as coatings or transitional layers aiming to bridge components with drastically different material properties. As a result, an FGM component is best designed as a coating perfectly bonded to a supporting layer. Additional mathematical efforts required in the semianalytical formulation of such a three-layer structure, however, are massive. The major difficulties include the determination of coefficient functions in Fourier transforms of displacements and stresses and the numerical integration of the resultant singular integral equations. For axisymmetric problems Fourier transforms must also be replaced by Hankel ones. For these reasons, semianalytical solutions to a receding contact occurring in structures composed of more than two layers are relatively rare (Adibelli *et al.* 2013, Yaylacı and Birinci 2013, Yaylacı *et al.* 2014), not to mention those containing FGM coatings (Yan and Mi 2017a, b).

Given the often intimidating mathematical difficulties involved in theoretical analysis, researchers have also resorted to finite element (FE) modeling, an accurate and robust numerical method, to solve receding contact problems. Kauzlarich and Greenwood (2001) numerically solved the receding contact radius between a pad and a rigid/elastic support due to an axisymmetric load by a three-dimensional FE modeling. Their results are found in good agreement with the semianalytical predictions by Keer *et al.* (1972). Öner *et al.* (2014) solved the receding contact problem between two unbonded elastic layers of finite thickness supported by a Winkler foundation using both the analytical method and an FE modeling. Nearly perfect agreement was found between the results from two methods. The same group of authors further made a few extensions of the classical receding contact model by comparing analytical and FE results (Yaylacı *et al.* 2014, Adiyaman *et al.* 2015, Birinci *et al.* 2015). Rončević and Siminiati (2010) performed FE modeling of the classical receding contact model using commercial software and successfully validated their numerical results against analytical solutions available in literature. Later, this work

was further extended to the receding contact between an elastic indenter and a homogeneous layer due to uniform pressure loads and this time the FE results are validated against experimental measurements based on digital image correlation technique (Rončević *et al.* 2016).

As can be seen from the above literature review on FE analysis of receding contact problems, most mechanical models are limited to homogeneous materials. When a structural element with graded properties are concerned, an FE model has to discretize the originally varying modulus of elasticity. In the semianalytical determination of the stress field around a cylindrical crack embedded inside the wall of a cylindrical tube, externally bonded to an infinite substrate and internally to a solid cylinder, Itou and Shima (1999) chose to divide the interfacial layer into three sublayers with the same thickness. Young's modulus and Poisson's ratio in each of the three sublayers are taken as constants, evaluated at sublayer lower surfaces. This idea of discretization has also found its applications in the FE modeling of structures containing FGM components. For example, Turan *et al.* (2016) developed an FE formulation for the advancing contact problem between an FGM layer and a half-space substrate, perfectly bonded along their interface, due to a uniform surface pressure applied on a circular portion of the top surface. FE results of displacements and stresses are able to be validated against those of classical elasticity. In a similar fashion, Balci *et al.* (2016) proposed an FE methodology for the thermoelastic contact problem of a thin FGM layer coated on a homogeneous half-plane substrate, indented by a sliding stamp. Also using a sliding stamp, Güler *et al.* (2017) recently developed an analytical and finite element comparative study on the plane contact over a functionally graded orthotropic half-plane. The FE modeling of an FGM layer involved in a receding contact structure, however, remains unelucidated.

In this paper, we aim to tackle the receding contact of a coated elastic layer pressed against a halfplane substrate by both a semianalytical and an FE modeling approach. The material properties of the coating are allowed to vary exponentially along the thickness direction. The indentation load is either a concentrated force or uniform compressive tractions acted upon the top surface of the composite laminate. The interface between the FGM layer and substrate is assumed frictionless such that no shear tractions can be transmitted. Both the semianalytical and FE analysis are performed within the framework of linear elasticity. The central result of the semianalytical formulation is a singular integral equation which is numerically integrated by Gauss-Chebyshev quadrature, together with the global force balance condition. An iterative algorithm based on the method of steepest descent is developed to guarantee the convergence of the solution. The key techniques of the FE modeling include the division of the FGM coating into homogeneous sublayers, smoothing of nodal stresses at sublayer interfaces, and the definition of receding contact at the FGM-substrate interface.

The remainder of this paper is organized as follows. Section 2 describes the semianalytical formulation of the proposed receding contact model, reinforced by a numerical integration algorithm tailored for the resultant singular

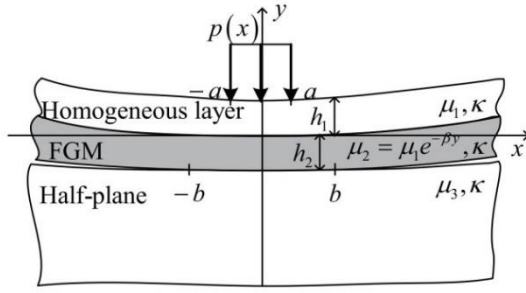


Fig. 1 Geometry of the receding contact problem between a two-layer inhomogeneous laminate and a half-plane substrate, pressed against each other due to a uniformly distributed surface traction

integral equation. In Section 3, the pre- and post-processing settings of FE contact modeling in the commercial software package ABAQUS/Standard are introduced such that the presented simulations can be independently repeated. Section 4 aims to validate the semianalytical solution against available literature results and FE modeling, to perform extensive parametric studies on receding contact parameters, and to discuss the significance of results predicted by both methods. Finally, in Section 5, conclusions of the paper are drawn and an outlook to future work foreseen.

## 2. Method of semianalytical solution

Let us consider an infinite two-layer laminate pressed against a half-plane substrate due to a uniformly distributed surface traction of intensity  $p(x)$ , as shown in Fig. 1. The laminate is composed of a homogeneous elastic layer of thickness  $h_1$  and a functionally graded one with thickness  $h_2$ . The elastic and FGM layers are perfectly bonded along their interface. The material properties of all three media are characterized by shear modulus  $\mu$  and Kolosov's constant  $\kappa$ . In the linear theory of plane elasticity, the latter parameter is a generalization of Poisson's ratio, i.e.,  $\kappa = 3 - 4\nu$  in plane strain formulation whereas  $\kappa = (3 - \nu)/(1 + \nu)$  for plane stress problems. For simplicity, the Kolosov's constant of all three media has been set to equal in the present study. While the elastic layer and the half-plane substrate are both treated as homogeneous media, the shear modulus of the FGM layer is allowed to vary exponentially along its transverse dimension

$$\mu_2(y) = \mu_1 e^{-\beta y}, \quad -h_2 \leq y < 0 \quad (1)$$

where  $\beta$  is an arbitrary nonzero constant. Neglecting gravity and friction at the FGM-substrate interface, the displacement equations of equilibrium for all three deformable media can be formulated as

$$(\kappa + 1) \frac{\partial^2 u_l}{\partial x^2} + (\kappa - 1) \frac{\partial^2 u_l}{\partial y^2} + 2 \frac{\partial^2 v_l}{\partial x \partial y} = 0 \quad (2a)$$

$$(\kappa - 1) \frac{\partial^2 v_l}{\partial x^2} + (\kappa + 1) \frac{\partial^2 v_l}{\partial y^2} + 2 \frac{\partial^2 u_l}{\partial x \partial y} = 0 \quad (2b)$$

$$\begin{aligned} & (\kappa + 1) \frac{\partial^2 u_2}{\partial x^2} + (\kappa - 1) \frac{\partial^2 u_2}{\partial y^2} + 2 \frac{\partial^2 v_2}{\partial x \partial y} \\ & - \beta(\kappa - 1) \frac{\partial u_2}{\partial y} - \beta(\kappa - 1) \frac{\partial v_2}{\partial x} \\ & = 0 \end{aligned} \quad (2c)$$

$$\begin{aligned} & (\kappa - 1) \frac{\partial^2 v_2}{\partial x^2} + (\kappa + 1) \frac{\partial^2 v_2}{\partial y^2} + 2 \frac{\partial^2 u_2}{\partial x \partial y} \\ & - \beta(3 - \kappa) \frac{\partial u_2}{\partial x} - \beta(\kappa + 1) \frac{\partial v_2}{\partial y} \\ & = 0 \end{aligned} \quad (2d)$$

It is clear that the first two equations of (2) work for the homogeneous elastic layer and half-plane substrate ( $l = 1$  or 3) whereas the last two for the infinite FGM lamina. The central task of a plane elastic problem is to seek a general solution to Eqs. (2). Such a solution is only general in the sense that it often contains arbitrary constants or functions that have to be determined by imposing the boundary conditions of a given mechanical model.

### 2.1 Mathematical formulation of the receding contact problem

The technique of standard Fourier transform is now implemented upon Eqs. (2a), (2b), (2c), (2d), since in the transformed space these partial differential equations can be converted into ordinary ones. For the elastic layer ( $0 \leq y \leq h_1$ ), the transformed displacements and stresses read

$$\tilde{u}_1(\lambda, y) = (C_1 + C_2 y) e^{\lambda y} + (C_3 + C_4 y) e^{-\lambda y} \quad (3a)$$

$$\begin{aligned} \tilde{v}_1(\lambda, y) = i \left[ \right. & \left. \left( C_1 + C_2 \left( y - \frac{\kappa}{\lambda} \right) \right) e^{\lambda y} \right. \\ & \left. - \left( C_3 + C_4 \left( y + \frac{\kappa}{\lambda} \right) \right) e^{-\lambda y} \right] \end{aligned} \quad (3b)$$

$$\begin{aligned} \tilde{\sigma}_{yy1}(\lambda, y) = 2\mu_1 i \left[ \right. & \left. \left( C_1 \lambda - C_2 \left( \frac{1 + \kappa}{2} - \lambda y \right) \right) e^{\lambda y} \right. \\ & \left. + \left( C_3 \lambda + \left( \frac{1 + \kappa}{2} + C_4 \lambda y \right) \right) e^{-\lambda y} \right] \end{aligned} \quad (4a)$$

$$\begin{aligned} \tilde{\sigma}_{xy1}(\lambda, y) = 2\mu_1 \left[ \right. & \left. \left( C_1 \lambda + C_2 \left( \frac{1 - \kappa}{2} + \lambda y \right) \right) e^{\lambda y} \right. \\ & \left. - \left( C_3 \lambda - C_4 \left( \frac{1 - \kappa}{2} - \lambda y \right) \right) e^{-\lambda y} \right] \end{aligned} \quad (4b)$$

where  $C_1$  through  $C_4$  are arbitrary functions of  $\lambda$ , namely the transform of the spatial variable  $x$ . These functions are taken as unknowns and can be solved by enforcing boundary conditions. The transformed displacements and stresses for the FGM layer ( $h_2 \leq y \leq 0$ ) appear in a much more complicated form, due to its inhomogeneous distribution of elastic modulus

$$\tilde{u}_2(\lambda, y) = \sum_{k=1}^4 C_{k+4} e^{m_k y} \quad (5a)$$

$$\tilde{v}_2(\lambda, y) = \sum_{k=1}^4 C_{k+4} n_k e^{m_k y} \quad (5b)$$

$$\tilde{\sigma}_{yy2}(\lambda, y) = \frac{\mu_2 e^{-\beta y}}{\kappa - 1} \sum_{k=1}^4 C_{k+4} [(1 + \kappa) m_k n_k - i(3 - \kappa)\lambda] e^{m_k y} \quad (6a)$$

$$\tilde{\sigma}_{xy2}(\lambda, y) = \mu_2 e^{-\beta y} \sum_{k=1}^4 C_{k+4} [m_k - i\lambda n_k] e^{m_k y} \quad (6b)$$

where  $m_1, \dots, m_4$  and  $n_1, \dots, n_4$  are known functions of  $\lambda$ , given in Appendix A. As before,  $C_5, \dots, C_8$  are also unknown functions of  $\lambda$  that have to be solved from the boundary conditions. The semiinfinite nature of the half-plane substrate requires that both displacements and stresses must vanish in regions far away from the area of receding contact. This condition helps to simplify the Fourier transforms of the elastic fields in the half-plane substrate and to reduce the number of unknown functions from four to two

$$\tilde{u}_3(\lambda, y) = (C_9 + C_{10}y) e^{|\lambda|y} \quad (7a)$$

$$\tilde{v}_3(\lambda, y) = i \left[ C_9 \operatorname{sgn}(\lambda) + C_{10} \left( y \operatorname{sgn}(\lambda) - \frac{\kappa}{\lambda} \right) \right] e^{|\lambda|y} \quad (7b)$$

$$\begin{aligned} \tilde{\sigma}_{yy3}(\lambda, y) = & 2i\mu_3 \left[ C_9 \lambda \right. \\ & \left. + C_{10} \left( \lambda y - \frac{(1 + \kappa)}{2} \operatorname{sgn}(\lambda) \right) \right] e^{|\lambda|y} \end{aligned} \quad (8a)$$

$$\tilde{\sigma}_{xy3}(\lambda, y) = 2\mu_3 \left[ C_9 |\lambda| + C_{10} \left( \frac{1 - \kappa}{2} + |\lambda|y \right) \right] e^{|\lambda|y} \quad (8b)$$

where  $\operatorname{sgn}(\lambda)$  is the signum function of  $\lambda$ .

Under the application of the uniformly distributed surface loads acting upon only a segment of the upper surface of the elastic layer, the traction boundary conditions are straightforward

$$\sigma_{yy1}(x, h_1) = -p(x)H(a - |x|), \quad |x| < \infty \quad (9a)$$

$$\sigma_{xy1}(x, h_1) = 0, \quad |x| < \infty \quad (9b)$$

where  $H(a - |x|)$  is the unit step function and  $a$  the half-length of the uniform surface traction. It is noted that in the present study the surface traction  $p(x)$  is given a priori, which helps to simplify the mathematical efforts.

Perfect bonding at the interface separating the elastic and FGM layer renders us both continuous displacements and stresses

$$\sigma_{yy1}(x, 0) = \sigma_{yy2}(x, 0), \quad |x| < \infty \quad (10a)$$

$$\sigma_{xy1}(x, 0) = \sigma_{xy2}(x, 0), \quad |x| < \infty \quad (10b)$$

$$u_1(x, 0) = u_2(x, 0), \quad |x| < \infty \quad (10c)$$

$$v_1(x, 0) = v_2(x, 0), \quad |x| < \infty \quad (10d)$$

Without friction, only compressive normal tractions can be transmitted across the area of receding contact

$$\sigma_{yy2}(x, -h_2) = -q(x)H(b - |x|), \quad |x| < \infty \quad (11a)$$

$$\sigma_{xy2}(x, -h_2) = 0, \quad |x| < \infty \quad (11b)$$

$$\sigma_{yy3}(x, -h_2) = -q(x)H(b - |x|), \quad |x| < \infty \quad (11c)$$

$$\sigma_{xy3}(x, -h_2) = 0, \quad |x| < \infty \quad (11d)$$

where  $q(x)$  denotes the receding contact pressure and  $b$  the contact half-length.

Three groups of boundary conditions, i.e., Eqs. (9a), (9b), (10a), (10b), (10c), (10d), (11a), (11b), (11c), (11d), provide ten equations to solve for the same number of unknown functions ( $C_1, \dots, C_{10}$ ). It is fortunate that these equations are all linear with respect to the ten unknowns. To this end, we substitute the transformed displacements and stresses (3a), (3b), (4a), (4b), (5a), (5b), (6a), (6b), (8a), (8b) into the Fourier transforms of the above three groups of boundary conditions. Although the procedure is logically straightforward yet mathematically quite tedious. For brevity, the solutions to these functions ( $C_1, \dots, C_{10}$ ) are documented in Appendix B.

Up to this point, the elastic field in all three media is symbolically solved. However, both the receding contact pressure and contact length at the FGM-substrate interface remain unknown. Recall that, as long as the condition of continuous contact is satisfied no gaps should be found across the FGM-substrate interface

$$\frac{\partial v_2(x, -h_2)}{\partial x} = \frac{\partial v_3(x, -h_2)}{\partial x}, \quad |x| < b \quad (12)$$

The displacement continuity condition has been formulated in terms of the interface slope in order to eliminate possible rigid-body movements. In addition, static equilibrium dictates that the resultant force of the contact pressure at the receding contact interface must balance that of the applied surface traction

$$\int_{-b}^b q(t) dt = \int_{-a}^a p(t) dt \quad (13)$$

Eqs. (12) and (13) are nothing but the conditions to determine the receding contact parameters. Plugging Eqs. (24a), (24b), (24c) back into the vertical displacements (5b), (7b) and subsequently imposing the slope continuity condition (12), a singular integral equation can be obtained

$$\begin{aligned} b_0 \int_{-b}^b q(t) \left\{ \frac{1}{t-x} + \int_0^\infty \sin[\lambda(t-x)] B(\lambda) d\lambda \right\} dt \\ = \frac{e^{\beta h_2}}{(1-\kappa)} \int_{-a}^a k(x, t) p(t) dt \end{aligned} \quad (14)$$

where

$$= \int_0^\infty \lambda \sin[\lambda(t-x)] \sum_{k=1}^4 (-1)^k \frac{D_{1(k+4)}}{D} n_k e^{-m_k h_2} d\lambda \quad (15a)$$

$$B(\lambda) = \frac{\lambda}{b_0} \sum_{k=1}^4 (-1)^k \frac{D_{7(k+4)}}{D} n_k e^{-m_k h_2} + \frac{\mu_1(1+\kappa)e^{\beta h_2}}{4\mu_3(\kappa-1)} - 1 \quad (15b)$$

and for very large  $\lambda$  expression (15b) can be further simplified by performing an asymptotic analysis (El-Borgi *et al.* 2006, White 2010)

$$b_0 = \frac{(1+\kappa)(e^{\beta h_2} \mu_1 + \mu_3)}{4\mu_3(\kappa-1)} \quad (16)$$

The singular integral Eq. (14) and the force balance Eq. (13) are the central conditions for determining the receding contact pressure  $q(x)$  and contact half-length  $b$ , whose semianalytical solution algorithm is outlined in the next subsection.

### 2.2 Semianalytical solution algorithm

One successful quadrature that can be used to numerically discretize the singular integral Eq. (14) is Gauss-Chebyshev formula (Erdogan and Gupta 1972, Li 2013). The integrals over  $[-b, b]$  and  $[-a, a]$  must both be changed into an integral over  $[-1, 1]$  before applying the quadrature rule. This change of intervals can be performed straightforwardly. In the meantime, we also choose to make the nondimensionalization  $x/b \rightarrow r$ . As a result, the singular integral Eq. (14) and the force balance condition (13) are converted to

$$b_0 \int_{-1}^1 \bar{q}(s) \left\{ \frac{1}{s-r} + b \int_0^\infty \sin[b\lambda(s-r)] B(\lambda) d\lambda \right\} ds = \frac{ae^{\beta h_2}}{(1-\kappa)} \int_{-1}^1 \bar{k}(r,s) \bar{p}(s) ds, \quad |r| \leq 1 \quad (17a)$$

$$b \int_{-1}^1 \bar{q}(s) ds = a \int_{-1}^1 \bar{p}(s) ds \quad (17b)$$

where

$$\bar{k}(r,s) = \int_0^\infty \lambda \sin[\lambda(as - br)] \sum_{k=1}^4 (-1)^k \frac{D_{1k+4}}{D} n_k e^{-m_k h_2} d\lambda \quad (18a)$$

$$\bar{q}(s) = h_1 q(bs)/P, \bar{p}(s) = h_1 p(as)/P \quad (18b, c)$$

with  $P$  representing the resultant force of the applied surface traction. Following Erdogan and Gupta (1972), the zeros of Chebyshev polynomial of the second kind are used as abscissae for quadratures. Moreover, Eq. (17a) was repeatedly evaluated at the zeros of Chebyshev polynomial of the first kind. This scheme leads to the following simultaneous algebraic equations for the receding contact half-length and the nondimensionalized contact pressure

$$b_0 \sum_{k=1}^N \bar{q}(s_j) \sqrt{1-s_j^2} \left\{ \frac{1}{s_j-r_i} + b \int_0^\infty \sin[b\lambda(s_j-r_i)] B(\lambda) d\lambda \right\} = \frac{ae^{\beta h_2}}{(1-\kappa)} \sum_{k=1}^N \bar{p}(s_j) \sqrt{1-s_j^2} \bar{k}(r_i, s_j) \quad (19a)$$

$$b \sum_{k=1}^N \bar{q}(s_j) \sqrt{1-s_j^2} = a \sum_{k=1}^N \bar{p}(s_j) \sqrt{1-s_j^2} \quad (19b)$$

where

$$r_i = \cos\left(\frac{\pi 2i-1}{2N+1}\right), \quad i = 1, \dots, N+1 \quad (20a)$$

$$s_j = \cos\left(\frac{j\pi}{N+1}\right), \quad j = 1, \dots, N \quad (20b)$$

are zeros of the  $(N+1)$  th degree Chebyshev polynomial of the first kind and the  $N$ th degree Chebyshev polynomial of the second kind, respectively.

Due to symmetry, the singular integral equation (17a) is identically satisfied at the midpoint of the receding contact length ( $r=0$ ). Consequently, it is more convenient to pick an even number for  $N$  such that the median equation of (19a), when  $i=N/2+1$ , can be dropped (Erdogan and Gupta 1972). As a result, Eqs. (19a), (19b) yield a total number of  $N+1$  equations for the same number of unknowns, i.e., the normalized contact pressure  $\bar{q}(s_j)$  and the contact half-length  $b$ . It is obvious that these algebraic equations are nonlinear for the contact half-length yet fortunately linear for the contact pressure. To solve for this pair of receding contact parameters, we first make a guess at  $b$  and subsequently evaluate  $\bar{q}$  from (19a). Next, the residual of (19b) is examined against a predefined degree of tolerance, e.g.,  $10^{-5}$ . Unless this tolerance condition is satisfactorily met, the guess of  $b$  must be renewed, by following the method of steepest descent (Ortega and Rheinboldt 1987), and the algorithm loop recycled.

### 3. Contact modeling in ABAQUS/Standard

For comparison purpose, the structure used in FE modeling is completely based on the model shown in Fig. 1. Benefiting from the symmetry, only a half of the theoretical model needs to be analyzed. The symmetry condition implies that at the center of the receding contact interface the horizontal displacement and the slope must satisfy

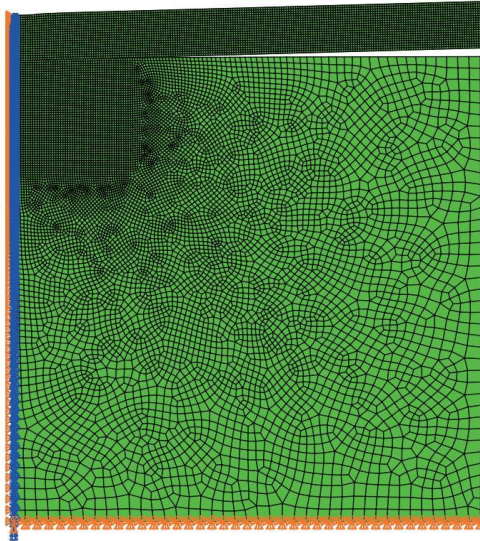


Fig. 2 Plane strain mesh details of the right half of the receding contact model under the application of uniform surface loads

Table 1 The discrete distribution of Young's modulus (GPa) in ten sublayers of a soft, nearly homogeneous, and hard FGM lamina. The Young's modulus of the homogenous elastic layer is assumed as  $E = 210$  GPa, the value of a typical steel material, such that the continuity at the elastic layer-FGM interface is guaranteed

sublayer	interval ( $h_2$ )	$\beta = -1$	$\beta = 0.001$	$\beta = 1$
1	0.0~ - 0.1	190.02	210	232.09
2	-0.1~ - 0.2	171.93	210	256.49
3	-0.2~ - 0.3	155.57	210	283.47
4	-0.3~ - 0.4	140.77	210	331.28
5	-0.4~ - 0.5	127.37	210	346.23
6	-0.5~ - 0.6	115.25	210	382.64
7	-0.6~ - 0.7	104.28	210	422.89
8	-0.7~ - 0.8	94.36	210	467.36
9	-0.8~ - 0.9	85.38	210	516.52
10	-0.9~ - 1.0	77.25	210	570.84

$$u_x = \frac{\partial u_y}{\partial x} = 0, \quad x = 0, y \leq h_1 \quad (21)$$

The material properties of all three deformable media are defined as isotropic and linearly elastic. The receding contact problem is numerically analyzed in ABAQUS/Standard, a highly accurate linear and nonlinear implicit solver. The model is meshed with plane strain finite elements, i.e., CPE4I, namely the 4-node bilinear quadrilateral and incompatible modes. This element type can effectively avoid shear locking. In particular, for bending problems only a few number of elements are needed in the transverse dimension, in order to achieve the same accuracy as that of 8-node biquadratic elements. Noticeably, the computational cost is much less expensive.

Fig. 2 shows a referential geometry of the FE models analyzed in this work. Meshes in the vicinity of the area of

receding contact, where accuracy is of most importance, are finer than the rest of the domain. For regions away from the contact area, the advancing-front technique was used for mesh generation, such that meshes are evenly ramped. No significant stresses and deformation are expected in regions far away from the contact area. For the referential model shown in Fig. 2, the thickness of the elastic layer is chosen as the fundamental characteristic length. The thickness of the FGM layer is set to the same as that of the elastic layer  $h_2 = h_1$ . In theoretical analysis, the elastic layer, FGM lamina and half-plane substrate are all infinite in the horizontal dimension. Convergence tests demonstrate that for half-lengths longer than 20 times of  $h_1$ , FE analysis results are unaffected. The height of the substrate is also taken as  $20h_1$ . The surface traction is prescribed as uniformly distributed pressure on the upper surface of the elastic layer.

One of the key difficulties in the FE modeling of FGMs lies in the way how to handle the inhomogeneous distribution of material properties, since they are typically treated as constants in individual elements. In the calculation of the stress field around a cylindrical crack embedded in a cylindrical shell, whose Young's modulus and Poisson's ratio are assumed to vary linearly between those of an inscribed solid cylinder and those of a surrounding substrate, Itou and Shima (1999) chose to divide the interfacial cylindrical layer into three sublayers. Each sublayer was assigned distinct but constant elastic constants. In a similar fashion, we choose to divide the FGM layer into ten sublayers of equal thickness. As an example, Table 1 tabulates the values of Young's modulus in each of the ten sublayers, evaluated from Eq. (1) at sublayer lower surfaces with  $\mu_1 = 84$  GPa. For  $\nu = 0.25$  ( $\kappa = 2$  for plane strain), the corresponding Young's modulus reads  $E_1 = 210$  GPa, approximately the value of a typical steel component. In addition, the modulus of elasticity of the substrate is set to the same value as that in the homogeneous layer for the referential model ( $\mu_3 = \mu_1$ ). Furthermore, to remove the discontinuity of stresses at the interfaces between each pair of neighboring sublayers, the stresses at any node lying on sublayer interfaces are smoothed as the average of those obtained in four surrounding elements.

Another key step in the FE analysis of the present problem is the definition of contact. At the interface of receding contact, the stiffer one between the FGM layer and the substrate is always chosen as the master surface. The other one is called the slave surface. ABAQUS/Standard provides two discretization methods for defining contact, i.e. node-to-surface and surface-to-surface. In the former mode, master surface nodes are allowed to penetrate into the slave surface, but not vice versa. In this work, we adopted the surface-to-surface mode to define contact, in which the distance between the master and slave surface is constantly checked against a predefined (default) value. Two surfaces are artificially bonded if their distance becomes less than the tolerance. Otherwise, either a gap still exists or penetration has occurred. For larger tolerances, penetration is less likely to happen. However, both the computational cost and even the convergence can be threatened. Finally, in sliding formulation finite sliding was

Table 2 Validation of the semianalytical solution algorithm against existing results for the case of a concentrated surface load ( $a/h = 0.01$ ), with reference to the degenerated model given in El-Borgi *et al.* (2006)

$\beta h_2$	$b/h_2$	Error (El-Borgi <i>et al.</i> 2006)	Error (present)
-1	1.1778	2.0E-07	7.44E-05
0.001	1.3243	2.0E-07	9.24E-06
1	1.6026	2.0E-07	7.16E-06

assumed between the master and slave surfaces such that the extent of contact can be instantaneously receded with the application of increasing indentation loading.

#### 4. Results and discussion

##### 4.1 Comparison with literature results

It is instructive to first validate the proposed semianalytical solution algorithm against available literature results. The model investigated in the present work, as shown in Fig. 1, can be viewed as an extension to the one solved in El-Borgi *et al.* (2006). They calculated the receding contact half-length and contact pressure between an FGM layer of finite thickness  $h$  and a half-plane substrate, under the application of either a concentrated surface load, approximated by the uniform traction  $a/h = 0.01$ , or uniformly distributed surface tractions ( $a/h = 1, 2, 4$ ). The parameter  $a$  assumes the same meaning as in the present study, namely the half-length of the applied surface loads. It is seen that the model shown in Fig. 1 reduces to the degenerated one as studied in El-Borgi *et al.* (2006) when the homogeneous elastic layer is absent ( $h_1 = 0$ ) and changing the variable  $h_2 \rightarrow h_1$ .

The first three columns of Table 2 are directly adapted from the Table 1 of El-Borgi *et al.* (2006) for the particular case of a concentrated surface load, roughly approximated by the uniformly distributed surface traction with  $a/h = 0.01$ . Since the mechanical model of this type neglects any size effects that may appear at the nanoscale (Mi 2017), it is more convenient to perform the theoretical calculation under a dimensionless framework, i.e. Eqs. (19a-b). For this reason, the resultant force of the nondimensionalized surface traction is always kept a constant:  $\int_{-a/h}^{a/h} (hp(as)/P)ds = \int_{-a/h}^{a/h} \bar{p}(s)ds = 1$ . The fourth column represents the residual error of the force balance condition (19b), obtained in the present study by substituting the receding contact half-length (second column of Table 2) into Eqs. (19a), solving for the receding contact pressure  $q$ , and evaluating the absolute difference between two sides of (19b). Instead of directly comparing the receding contact parameters obtained in the present study and those found in the literature, this means of validation provides a more effective evaluation on the accuracy of the developed solution algorithm. In view of the data tabulated in Table 2, it can be concluded that excellent agreement has been achieved and thus the solution algorithm developed in previous sections are validated.

##### 4.2 Comparison between semi analytical solution and FE results

In this subsection, we present an analytical and FE comparative study on the receding contact stress and contact half-length at the FGM-substrate interface, as functions of the inhomogeneity index  $\beta h_2$  defined for the FGM layer and the relative distribution range of the surface traction  $a/h_1$ . Although the semianalytical analysis can be performed within the dimensionless framework, FE modeling requires a concrete mechanical model. The geometry of the FE model is constructed on the basis of the referential model discussed in Section 3: the thicknesses  $h_2 = h_1 = 1$ mm, the shear moduli  $\mu_3 = \mu_1 = 84$  GPa, the resultant force  $P = 1000$ N, Poisson's ratio  $\nu = 0.25$ , and Kolosov's constant  $\kappa = 2$  for plane strain condition. For a given ratio  $a/h_1$ , the surface traction applied on the FE model always satisfies the condition  $\int_{-a/h}^{a/h} (h_1 p(as)/P)ds = \int_{-a/h}^{a/h} \bar{p}(s)ds = 1$ . Therefore, the expression for a uniform surface traction reduces to:  $p(x) = P/(2a), |x| \leq a$  representing a line force of constant intensity.

Figs. 3 through 5 show the distribution of the dimensionless contact stress at the FGM-substrate interface due to a concentrated surface load  $a/h_1 = 0.01$ , a uniform surface traction  $a/h_1 = 1$ , and  $a/h_1 = 2$ , respectively. For each loading condition, a soft ( $\beta h_2 = -1$ ), a nearly homogeneous ( $\beta h_2 = 0.001$ ), and a hard ( $\beta h_2 = 1$ ) FGM layer are considered. Both the semianalytical solution (solid line) and the FE modeling results (black dots) are presented in the figures. As mentioned in Section 3, meshes with finer elements (0.1 mm) were used for the region close to the receding contact and were evenly ramped to coarser elements (0.5 mm) toward the remote boundaries of the model. For the case of a concentrated load (Fig. 3), even finer meshes (0.01 mm) have to be used for a small domain immediately beneath the loading area. Except the surface traction and the inhomogeneity index, the other parameters are all kept as constants, as explained above.

It is seen that the analytical solution and FE modeling results are able to validate against each other with a sufficient degree of accuracy. For all three surface tractions considered in this subsection, FE modeling slightly underestimates the level of contact stresses near the center and both perimeters of the area of receding contact. In other regions, both solutions are found in perfect agreement. It should also be noted that while the analytical solution is able to accurately predict the contact size up to three significant figures, FE modeling is much less competent, due to the discrete nature of FE method. Table 3 compares the receding contact half-lengths obtained by the semi analytical solution and FE analysis with two typical element sizes implemented in the finely meshed region, for the nine cases studied in Figs. 3 through 5. To be specific, the accuracy of FE analysis results is limited by the size of the plane strain elements adopted in the simulation. Consequently, when FE modeling is employed as a means of analyzing contact problem one should focus on the pressure distribution instead of the contact size.

Table 3 Comparison of the receding contact half-length  $b$  obtained by the semianalytical analysis and FE modeling with two typical element sizes (0.1 mm and 0.05 mm), for nine combinations of surface loads and FGM inhomogeneity index

$a/h_1$	$\beta h_2 = -1$			$\beta h_2 = 0.001$			$\beta h_2 = 1$		
	Anal.	FE(0.1)	FE(0.05)	Anal.	FE(0.1)	FE(0.05)	Anal.	FE(0.1)	FE(0.05)
0.01	2.3620	2.4	2.35	2.6540	2.7	2.65	3.1112	3.1	3.10
1	2.5827	2.6	2.60	2.8715	2.9	2.85	3.3031	3.3	3.30
2	3.2100	3.2	3.20	3.4597	3.5	3.45	3.8340	3.8	3.85

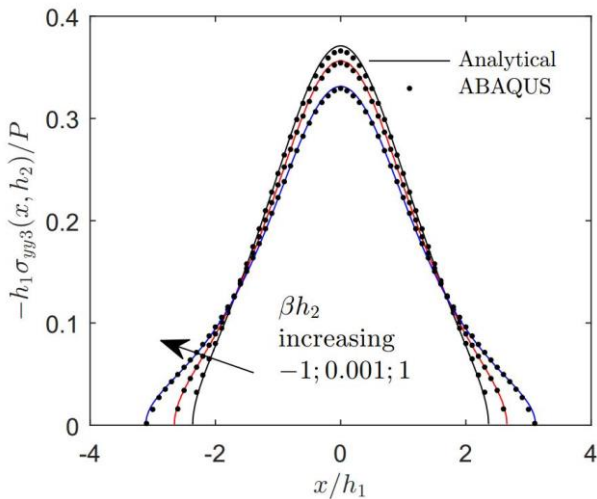


Fig. 3 Distribution of the receding contact stress at the FGM-substrate interface under the application of a concentrated surface load ( $a/h_1 = 0.01$ ,  $h_2/h_1 = 1$ ,  $\mu_3/\mu_1 = 1$ ,  $\int_{-a/h_1}^{a/h_1} \bar{p}(s)ds = 1$ )

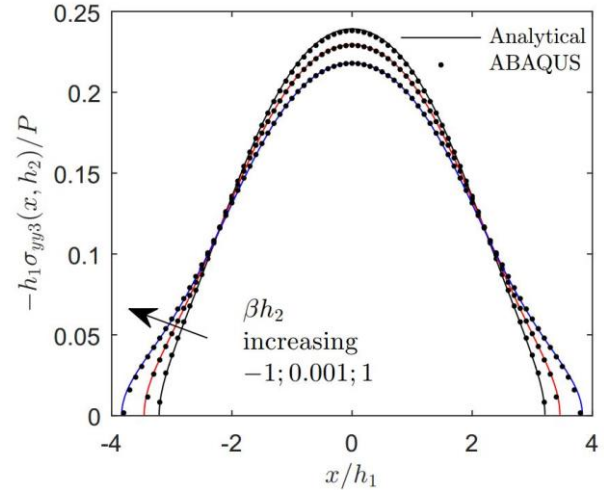


Fig. 5 Distribution of the receding contact stress at the FGM-substrate interface under the application of a uniformly distributed surface traction ( $a/h_1 = 2$ ,  $h_2/h_1 = 1$ ,  $\mu_3/\mu_1 = 1$ ,  $\int_{-a/h_1}^{a/h_1} \bar{p}(s)ds = 1$ )

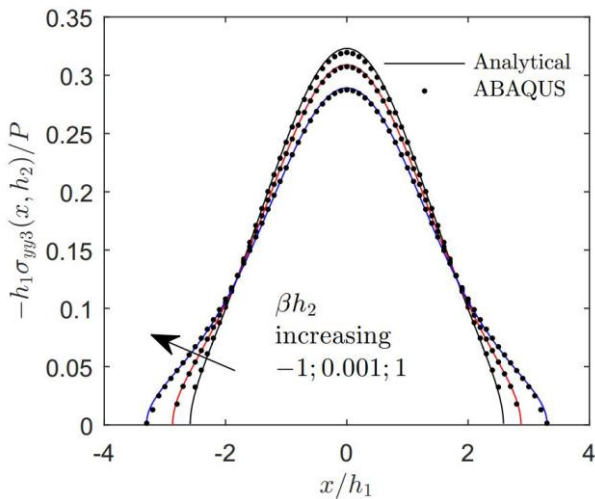


Fig. 4 Distribution of the receding contact stress at the FGM-substrate interface under the application of a uniformly distributed surface traction ( $a/h_1 = 1$ ,  $h_2/h_1 = 1$ ,  $\mu_3/\mu_1 = 1$ ,  $\int_{-a/h_1}^{a/h_1} \bar{p}(s)ds = 1$ )

Irrespective of the distribution property of surface tractions, the peak contact stress in Figs. 3-5 is always found at the center of the receding contact area and monotonically drop to zero at both perimeters. Under the application of a given surface traction, the peak contact

stress decreases with increasing FGM inhomogeneity index. The contact length, on the other hand, behaves an increasing function of the FGM inhomogeneity index. This observation is actually dictated by the force balance condition (13), since the area under any normalized stress curve must be equal to unity. Intersecting among the three curves in any plot are therefore inevitable.

A comparison among curves with the same inhomogeneity index in Figs. 3-5 reveals that the peak contact stress appears a decreasing function of the length scale ratio  $a/h_1$ . For contact length, the opposite conclusion is true. For the three types of surface tractions studied Figs. 3-5, the changes in both the peak stress and contact length are quite obvious, implying that the thickness of the composite laminate ( $h_1 + h_2$ ) are far shorter than enough to make the Saint-Venant's principle come into effect. As a result, both the contact pressure distribution and contact length must be determined on purpose for a particular surface load.

### 4.3 Semianalytical analysis results

Since the receding contact length can only be accurately captured in the theoretical modeling of the receding contact problem, this subsection devotes to the semianalytical analysis of the contact half-length  $b$  as a function of the surface traction property  $a/h_1$ , FGM inhomogeneity index

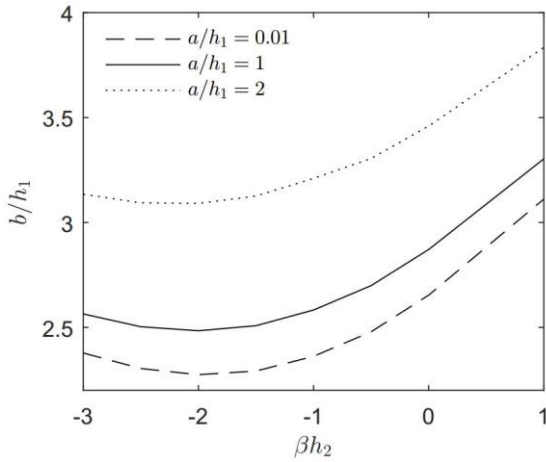


Fig. 6 Variation of the receding contact half-length as a function of the FGM inhomogeneity index for three types of surface loads ( $h_2/h_1 = 1$ ,  $\mu_3/\mu_1 = 1$ ,  $\int_{-a/h_1}^{a/h_1} \bar{p}(s)ds = 1$ )

$\beta h_2$ , shear moduli ratio  $\mu_3/\mu_1$ , and thickness ratio  $h_2/h_1$ . In view of the force balance condition (13), the other contact parameter, the peak contact pressure  $q_{max}$ , can be qualitatively inferred from its inverse relation with  $b$ .

Fig. 6 shows the variation of the receding contact half-length as a function of the FGM inhomogeneity index in the continuous interval  $[-3,1]$ , for three types of surface loads. It can be seen that for a hard FGM layer ( $\beta h_2 > 0$ ), the contact half-length behaves an increasing function for all three surface tractions, implying that a hard FGM layer helps to expand the area of receding contact. Moreover, the harder the FGM layer the steeper the contact half-length curve becomes. Consequently, hard FGM layers should be employed provided that the peak contact stress is of the primary concern. For soft FGM layers, the situation is more complicated. The dependence of contact half-length on the FGM inhomogeneity index is not monotonic. The minimum contact half-length occurs in the vicinity of  $\beta h_2 = -2$ . The specific value at the point of inflection depends on the extent of the applied surface traction. In the less likely occasion where a small contact size is desired a negative FGM inhomogeneity index close to  $\beta h_2 = -2$  is most ideal.

The elastic stiffness of the half-plane substrate is another important factor that affects the property of receding contact. In Fig. 7, the receding contact half-length is plotted against different shear moduli ratios between the substrate and the elastic layer. As before, three FGM inhomogeneity indices were considered in the analysis. The receding contact length behaves a monotonically decreasing function of the ratio  $\mu_3/\mu_1$  in the studied range, independent on the FGM layer stiffness. The receding contact half-length  $b$  narrows about 0.8 times of the elastic layer thickness  $h_1$  when the half-plane changes from a soft ( $\mu_3 = 0.5\mu_1$ ) substrate to a hard ( $\mu_3/\mu_1 = 1$ ) one. The peak contact stress, on the other hand, can be expected to increase with the shear moduli ratio  $\mu_3/\mu_1$ . The function of the FGM layer is the same as in the previous analysis. Hard FGM layers are capable of elevating the overall level of contact size in the entire interval of shear moduli ratio.

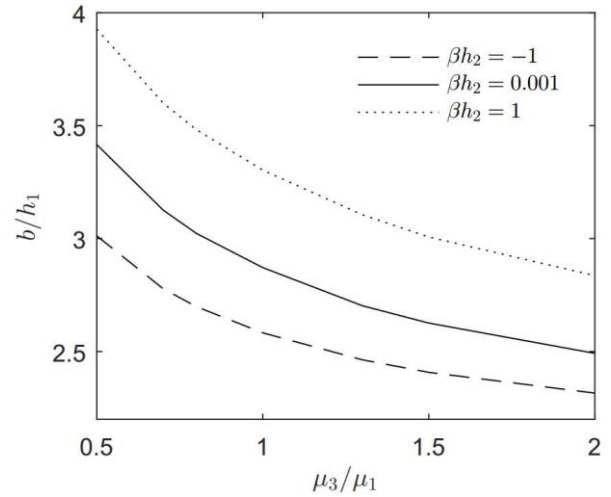


Fig. 7 Variation of the receding contact half-length as a function of the shear moduli ratio between the halfplane substrate and the homogeneous layer for three levels of FGM inhomogeneity index ( $a/h_1 = 1$ ,  $h_2/h_1 = 1$ ,  $\int_{-a/h_1}^{a/h_1} \bar{p}(s)ds = 1$ )

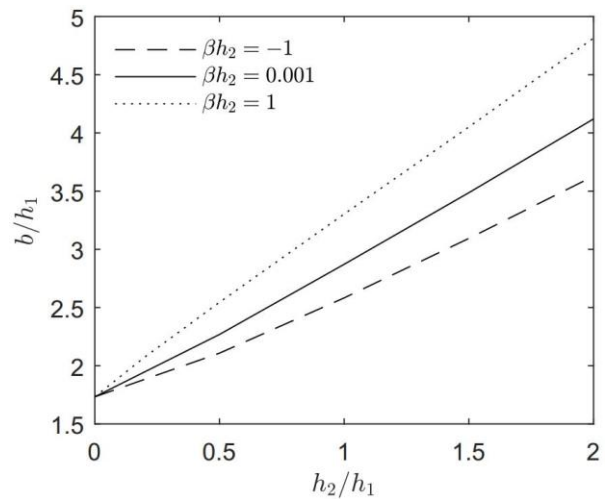


Fig. 8 Variation of the receding contact half-length as a function of the thickness ratio between the FGM and homogeneous layer for three levels of FGM inhomogeneity index ( $a/h_1 = 1$ ,  $\mu_3/\mu_1 = 1$ ,  $\int_{-a/h_1}^{a/h_1} \bar{p}(s)ds = 1$ )

We further studied the impact of the thickness ratio between the FGM and the elastic layer on the contact half-length for the uniform surface traction  $a/h_1 = 1$  (Fig. 8). As usual, three inhomogeneity indices were taken into account. The other parameters assume the same values as those defined for the referential model. For all three cases, the receding contact size appears nearly a linear function of the thickness ratio. This behavior implies that increasing the thickness ratio helps to expand the extent of receding contact and thus to reduce the peak contact stress. The rate of increase of the receding contact size, however, is a strong increasing function of the FGM inhomogeneity index. For the limiting case of  $h_2 = 0$ , the FGM layer is absent and therefore all three curves intersect at the same point as expected.

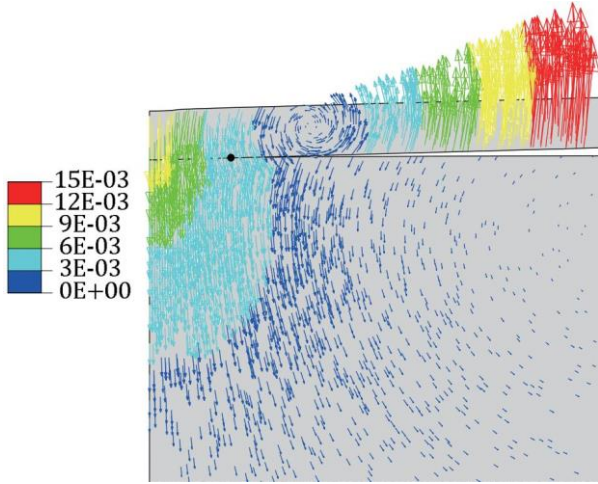


Fig. 9 Distribution of the nondimensionalized displacement vector  $\mathbf{u}/h_1$  near the area of receding contact. The black dot at the FGM-substrate interface denotes the boundary of the receding contact.  $a/h_1 = 1$ ,  $h_2/h_1 = 1$ ,  $\mu_3/\mu_1 = 1$ ,  $\beta h_2 = 1$ ,  $\int_{-a/h_1}^{a/h_1} \bar{p}(s) ds = 1$

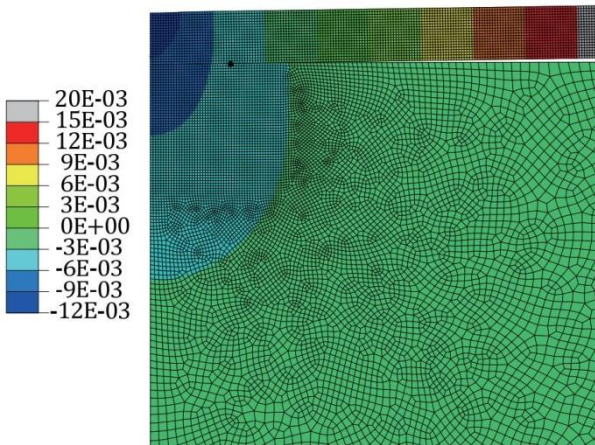


Fig. 10 Distribution of the nondimensionalized vertical displacement  $u_y/h_1$  near the area of receding contact. The black dot at the FGM-substrate interface denotes the boundary of the receding contact.  $a/h_1 = 1$ ,  $h_2/h_1 = 1$ ,  $\mu_3/\mu_1 = 1$ ,  $\beta h_2 = 1$ ,  $\int_{-a/h_1}^{a/h_1} \bar{p}(s) ds = 1$

#### 4.4 FE analysis results

Although FE analysis fails to accurately predict the receding contact half-length due to the limit of element size, it is able to generate the full-field displacements and stresses by a one-time calculation. In contrast, the determination of elastic field at regions other than the interface of receding contact encounters additional, often intimidating, challenges in a semi analytical solution. In this subsection, we present the FE results performed with respect to the referential model defined in Section 3:  $h_2 = h_1 = 1$  mm,  $\mu_3 = \mu_1 = 84$  GPa,  $P = 1000$  N, and  $\nu = 0.25$  ( $\kappa = 2$  for plane strain condition). In addition, the FGM inhomogeneity index is fixed as  $\beta h_2 = 1$ . The indentation load applied on the top surface of the elastic layer is a uniform surface traction of constant intensity

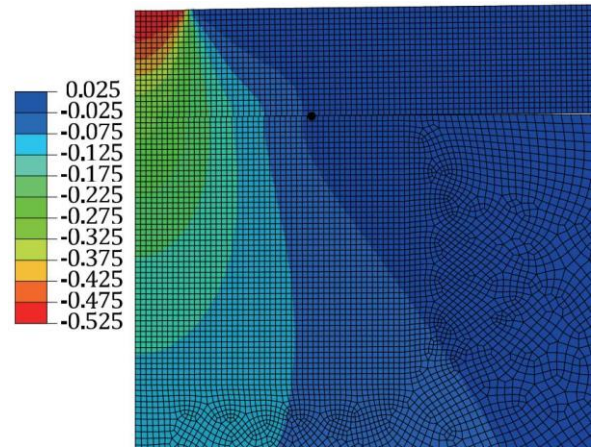


Fig. 11 Distribution of the nondimensionalized normal stress ( $h_1 \sigma_{yy}/P$ ) near the area of receding contact. The black dot at the FGM-substrate interface denotes the boundary of the receding contact.  $a/h_1 = 1$ ,  $h_2/h_1 = 1$ ,  $\mu_3/\mu_1 = 1$ ,  $\beta h_2 = 1$ ,  $\int_{-a/h_1}^{a/h_1} \bar{p}(s) ds = 1$

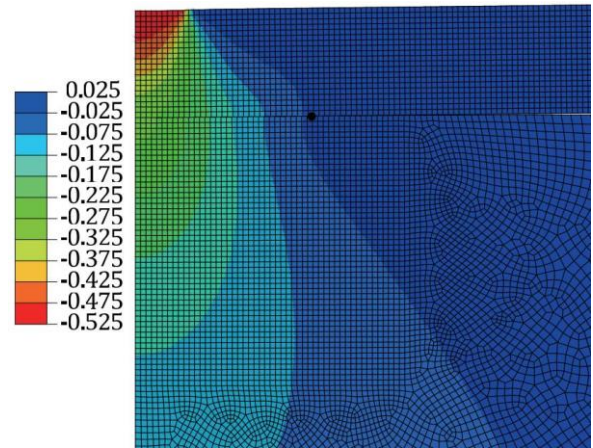


Fig. 11 Distribution of the nondimensionalized normal stress ( $h_1 \sigma_{yy}/P$ ) near the area of receding contact. The black dot at the FGM-substrate interface denotes the boundary of the receding contact.  $a/h_1 = 1$ ,  $h_2/h_1 = 1$ ,  $\mu_3/\mu_1 = 1$ ,  $\beta h_2 = 1$ ,  $\int_{-a/h_1}^{a/h_1} \bar{p}(s) ds = 1$

$p = P/(2a)$ , where  $a = h_1$ . The rest of the the top surface is traction free. All FE models were meshed with the same scheme as the one used for producing Fig. 4.

Fig. 9 represents the vector plot of the plane displacement field in the vicinity of the region of receding contact. For better illustrating the results, only a portion of the whole model is shown. Both the magnitude and direction of the displacements are plotted, illustrating the receding contact behavior occurring at the FGM layer-substrate interface under the application of the uniform surface traction. A displacement vortex is clearly observed around a point at the elastic-FGM layer interface, roughly twice the contact half-length measured from the symmetry axis. Across the center of the vortex, the direction of the displacement vector is reversed. For regions in  $x > 2b$ , the composite laminate is obviously deflected upward. The farther a field point is the larger the deflection becomes,

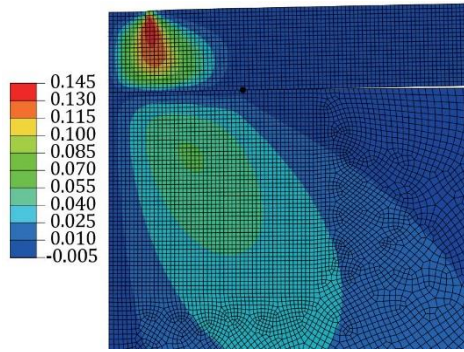


Fig. 12 Distribution of the nondimensionalized shear stress ( $h_1 \sigma_{xy}/P$ ) near the area of receding contact. The black dot at the FGM-substrate interface denotes the boundary of the receding contact.  $a/h_1 = 1$ ,  $h_2/h_1 = 1$ ,  $\mu_3/\mu_1 = 1$ ,  $\beta h_2 = 1$ ,  $\int_{-a/h_1}^{a/h_1} \bar{p}(s) ds = 1$

reflecting the receding nature of the composite laminate. Nonetheless, most of the displacements were contributed by rigid-body movements. A moderate level of downward deflection is found in regions near the area of receding contact. The major contribution comes from strain deformation, with the maximum value lying directly along the axis of symmetry. The displacement field in the substrate becomes negligibly small in the domain far away from the contact area, as denoted by those blue arrows in the lower-right corner of Fig. 9. Arguments regarding the direction of the displacements can also be confirmed from the nephogram of vertical displacement component, as shown in Fig. 10. The center of the displacement vortex is clearly a critical point across which the vertical displacement reverses its sign.

Figs. 11 and 12 show the distribution of normal ( $\sigma_{yy}$ ) and shear ( $\sigma_{xy}$ ) stress components near the area of receding contact, respectively. As mentioned in Section 3, in FE analysis the FGM layer is modeled by ten sublayers, each assigned by a distinct but constant modulus of elasticity (Table 1). As a result, stresses inevitably lose continuity across the interfaces separating individual sublayers. In the post-processing of FE results, the stress value of an interfacial node is assigned as the average value of four neighboring quadrilateral elements that share the node. In this way the nodal stress is smoothed and the continuity of stresses at the sublayer interfaces are guaranteed.

As can be expected, maximum normal stresses occur along the axis of symmetry, particularly in the inhomogeneous composite. For regions away from the  $y$  axis, the normal stress component quickly drop to zero (Fig. 11). The shear stress, on the other hand, shows a drastically different distribution. For the composite laminae, significant shear stresses appear in regions approximately below the perimeter of the applied uniform surface traction. The shear stress component in the substrate is most significant in the area directly underneath the boundary of the receding contact. This difference should be instructive, provided that the shear strength of such a multilayered structure is of the primary concern.

## 5. Conclusions

In this paper, we performed a comparison study on the receding contact between an inhomogeneous laminate and a half-plane substrate, pressed against each other by uniform surface tractions. The composite laminate is composed of a homogeneous elastic and an FGM layer, perfectly bonded along their interface. The receding contact pressure and contact length were solved by both a semianalytical approach and an FE modeling implemented in commercial software ABAQUS/Standard. By employing the standard Fourier transform technique, the former method converted the governing equations and boundary conditions of the problem into a singular integral equation which is then numerically integrated by Gauss-Chebyshev quadrature. In FE modeling, the FGM strip was modeled by a number of sublayers with distinct and constant modulus of elasticity and the nodal stresses on sublayer interfaces were averaged over surrounding elements in post-processing. In addition, the surface-to-surface discretization method and finite sliding formulation were adopted. A few observations and conclusions can be inferred from the extensive parametric studies implemented in both methods.

- The semianalytical solution and FE analysis results successfully validated against each other with high accuracy, indicating the effectiveness of both the semianalytical solution algorithm and the proposed FE pre- and post-processing techniques.

- For the three-layer structure proposed in Fig. 1, the most important contact parameter, namely the peak pressure, behaves a decreasing function of the FGM inhomogeneity index in the interval  $[-1 \leq \beta h_2 \leq 1]$ . The opposite is true for the receding contact length. A point of inflection, however, is found near  $\beta h_2 = -2$ . In addition, soft substrates, thick FGM layers and widening the coverage of statically equivalent surface tractions all help to reduce the peak contact pressure.

- The semianalytical solution algorithm is able to accurately predict the receding contact parameters, particularly the contact length, whereas FE modeling is good at determining the panoramic elastic field of the whole structure without additional efforts. The interesting course of contact loss between the composite laminate and the half-plane substrate is revealed by a vector plot of the displacement field.

The present study primarily focuses on the comparative study of the receding contact in a concrete three-layer inhomogeneous structure. Future work could entail the functional dependence of receding contact behavior in multilayered structures on more contributory factors such as the position of the FGM layer, substrates of finite thickness, friction, three-dimensional geometry, and the experimental validation of theoretical analysis and FE modeling.

## Acknowledgments

This work was supported by the National Natural Science Foundation of China (grant number 11472079), the

National Key R&D Program of China (grant number 2017YFC0702800), the Natural Science Foundation of Jiangsu Province (grant number BK20161411), and the Fundamental Research Funds for the Central Universities.

## References

- Adibelli, H., Çömez, İ. and Erdöl, R. (2013), "Receding contact problem for a coated layer and a half-plane loaded by a rigid cylindrical stamp", *Arch. Mech.*, **65**(3), 219-236.
- Adıyaman, G., Birinci, A., Öner, E. and Yaylacı, M. (2016), "A receding contact problem between a functionally graded layer and two homogeneous quarter planes", *Acta Mech.*, **227**(6), 1753-1766.
- Adıyaman, G., Öner, E. and Birinci, A. (2017), "Continuous and discontinuous contact problem of a functionally graded layer resting on a rigid foundation", *Acta Mech.*, **228**(9), 3003-3017.
- Adıyaman, G., Yaylacı, M. and Birinci, A. (2015), "Analytical and finite element solution of a receding contact problem", *Struct. Eng. Mech.*, **54**(1), 69-85.
- Balci, M.N., Dag, S. and Yildirim, B. (2016), "Subsurface stresses in graded coatings subjected to frictional contact with heat generation", *J. Therm. Stress.*, **40**(4), 517-534.
- Birinci, A., Adıyaman, G., Yaylacı, M. and Öner, E. (2015), "Analysis of continuous and discontinuous cases of a contact problem using analytical method and FEM", *Lat. Am. J. Sol. Struct.*, **12**(9), 1771-1789.
- Civelek, M. and Erdogan, F. (1974), "The axisymmetric double contact problem for a frictionless elastic layer", *Int. J. Sol. Struct.*, **10**(6), 639-659.
- Çömez, İ. (2010), "Frictional contact problem for a rigid cylindrical stamp and an elastic layer resting on a half plane", *Int. J. Sol. Struct.*, **47**(7-8), 1090-1097.
- Çömez, İ., Birinci, A. and Erdöl, R. (2004), "Double receding contact problem for a rigid stamp and two elastic layers", *Eur. J. Mech. A-Sol.*, **23**(2), 301-309.
- Çömez, İ., El-Borgi, S., Kahya, V. and Erdöl, R. (2016), "Receding contact problem for two-layer functionally graded media indented by a rigid punch", *Acta Mech.*, **227**(9), 2493-2504.
- El-Borgi, S., Abdelmoula, R. and Keer, L. (2006), "A receding contact plane problem between a functionally graded layer and a homogeneous substrate", *Int. J. Sol. Struct.*, **43**(3-4), 658-674.
- El-Borgi, S., Usman, S. and Güler, M.A. (2014), "A frictional receding contact plane problem between a functionally graded layer and a homogeneous substrate", *Int. J. Sol. Struct.*, **51**(25-26), 4462-4476.
- Erdogan, F. and Gupta, G.D. (1972), "On the numerical solution of singular integral equations", *Q. Appl. Math.*, **29**(4), 525-534.
- Erdogan, F. and Ratwani, M. (1974), "The contract problem for an elastic layer supported by two elastic quarter planes", *J. Appl. Mech.*, **41**(3), 673-678.
- Gecit, M.R. (1986), "Axisymmetric contact problem for a frictionless elastic layer indented by an elastic cylinder", *Comput. Mech.*, **1**(2), 91-104.
- Güler, M.A., Kucuksucu, A., Yilmaz, K.B. and Yildirim, B. (2017), "On the analytical and finite element solution of plane contact problem of a rigid cylindrical punch sliding over a functionally graded orthotropic medium", *Int. J. Mech. Sci.*, **120**, 12-29.
- Itou, S. and Shima, Y. (1999), "Stress intensity factors around a cylindrical crack in an interfacial zone in composite materials", *Int. J. Sol. Struct.*, **36**(5), 697-709.
- Johnson, K.L. (1985), *Contact Mechanics*, Cambridge University Press, London, U.K.
- Kauzlarich, J.J. and Greenwood, J.A. (2001), "Contact between a centrally loaded plate and a rigid or elastic base, with application to pivoted pad bearings", *P. I. Mech. Eng. C-J. Mec.*, **215**(6), 623-628.
- Keer, L.M. and Chantaramungkorn, K. (1972), "Loss of contact between an elastic layer and half-space", *J. Elast.*, **2**(3), 191-197.
- Keer, L.M., Dundurs, J. and Tsai, K.C. (1972), "Problems involving a receding contact between a layer and a half space", *J. Appl. Mech.*, **39**(4), 1115-1120.
- Li, X. (2013), *Integral Equations, Boundary Value Problems and Related Problems*, World Scientific Publishing, Singapore.
- Mi, C. (2017), "Surface mechanics induced stress disturbances in an elastic half-space subjected to tangential surface loads", *Eur. J. Mech. A-Sol.*, **65**, 59-69.
- Öner, E., Yaylacı, M. and Birinci, A. (2014), "Solution of a receding contact problem using an analytical method and a finite element method", *J. Mech. Mater. Struct.*, **9**(3), 333-345.
- Ortega, J.M. and Rheinboldt, W.C. (1987), *Iterative Solution of Nonlinear Equations in Several Variables*, Society for Industrial and Applied Mathematics, Philadelphia, U.S.A.
- Parel, K. and Hills, D. (2016), "Frictional receding contact analysis of a layer on a half-plane subjected to semi-infinite surface pressure", *Int. J. Mech. Sci.*, **108-109**, 137-143.
- Rhimi, M., El-Borgi, S. and Lajnef, N. (2011), "A double receding contact axisymmetric problem between a functionally graded layer and a homogeneous substrate", *Mech. Mater.*, **43**(12), 787-798.
- Rhimi, M., El-Borgi, S., Ben, S.W. and Jemaa, F.B. (2009), "A receding contact axisymmetric problem between a functionally graded layer and a homogeneous substrate", *Int. J. Sol. Struct.*, **46**(20), 3633-3642.
- Rončević, B. and Siminiati, D. (2010), "Two-dimensional receding contact analysis with NX Nastran", *Adv. Eng.*, **4**(1), 69-74.
- Rončević, B., Bakić, A. and Kodvanj, J. (2016), "Numerical and experimental analysis of a frictionless receding contact between cylindrical indenter, layer and substrate", *T. Famena*, **40**(2), 1-18.
- Tsai, K.C., Dundurs, J. and Keer, L.M. (1974), "Elastic layer pressed against a half space", *J. Appl. Mech.*, **41**(3), 703-707.
- Turan, M., Adıyaman, G., Kahya, V. and Birinci, A. (2016), "Axisymmetric analysis of a functionally graded layer resting on elastic substrate", *Struct. Eng. Mech.*, **58**(3), 423-442.
- White, R. (2010), *Asymptotic Analysis of Differential Equations*, Imperial College Press, Singapore.
- Yan, J. and Li, X. (2015), "Double receding contact plane problem between a functionally graded layer and an elastic layer", *Eur. J. Mech. A-Sol.*, **53**, 143-150.
- Yan, J. and Mi, C. (2017a), "Double contact analysis of multilayered elastic structures involving functionally graded materials", *Arch. Mech.*, **69**(3), 199-221.
- Yan, J. and Mi, C. (2017b), "On the receding contact between an inhomogeneously coated elastic layer and a homogeneous half-plane", *Mech. Mater.*, **112**, 18-27.
- Yaylacı, M. and Birinci, A. (2013), "The receding contact problem of two elastic layers supported by two elastic quarter planes", *Struct. Eng. Mech.*, **48**(2), 241-255.
- Yaylacı, M., Öner, E. and Birinci, A. (2014), "Comparison between analytical and ANSYS calculations for a receding contact problem", *J. Eng. Mech.*, **140**(9), 04014070.

## Appendix A

This appendix outlines the expressions of  $m_1, \dots, m_4$  and  $n_1, \dots, n_4$  introduced in Eqs. (5) and (6).

$$m_1(\lambda) = \frac{1}{2} \left( \beta + \sqrt{\beta^2 + 4\lambda^2 - 4i\beta\lambda \sqrt{\frac{3-\kappa}{1+\kappa}}} \right) \quad (22a)$$

$$m_2(\lambda) = \frac{1}{2} \left( \beta - \sqrt{\beta^2 + 4\lambda^2 - 4i\beta\lambda \sqrt{\frac{3-\kappa}{1+\kappa}}} \right) \quad (22b)$$

$m_3$  and  $m_4$  are complex conjugates of  $m_1$  and  $m_2$ , respectively, and

$$n_k(\lambda) = \frac{(\kappa-1)m_k^2 - \beta(\kappa-1)m_k - \lambda^2(\kappa+1)}{i\lambda(2m_k - \beta(\kappa-1))}, \quad k = 1, 2, 3, 4 \quad (23)$$

## Appendix B

In this appendix, we present the solutions to unknown functions  $C_1, \dots, C_{10}$  appeared in the Fourier transforms of displacements and stresses.

$$C_k(\lambda) = (-1)^k \left( \frac{D_{1k}}{D} \tilde{P} + \frac{D_{7k}}{D} \tilde{Q} \right), \quad k = 1, \dots, 8 \quad (24a)$$

$$C_9(\lambda) = \frac{(2|\lambda|h_2 - 1 + \kappa)\mu_1 e^{(|\lambda|+\beta)h_2}}{4i\lambda\mu_3(\kappa-1)} \tilde{Q} \quad (24b)$$

$$C_{10}(\lambda) = \frac{\mu_1 e^{(|\lambda|+\beta)h_2}}{2i\mu_3(\kappa-1)} \operatorname{sgn}(\lambda) \tilde{Q} \quad (24c)$$

where

$$\tilde{P}(\lambda) = \frac{1}{2\pi\mu_1} \int_{-a}^a p(t) e^{it\lambda} dt \quad (25a)$$

$$\tilde{Q}(\lambda) = \frac{\kappa-1}{2\pi\mu_1 e^{\beta h_2}} \int_{-b}^b q(t) e^{it\lambda} dt \quad (25b)$$

and  $D_{jk}$  is the determinant of the submatrix of

$$D = \begin{bmatrix} D' & O \\ O & D'' \end{bmatrix} \quad (26)$$

obtained by removing its  $j^{\text{th}}$  row and  $k^{\text{th}}$  column. In the block matrix  $D$ , both submatrices  $O$  represent a  $2 \times 4$  zero matrix and

$$D' = \begin{bmatrix} 2i\lambda e^{\lambda h_1} & -i(1+\kappa-2\lambda h_1)e^{\lambda h_1} & 2i\lambda e^{-\lambda h_1} & i(1+\kappa+2\lambda h_1)e^{-\lambda h_1} \\ 2\lambda e^{\lambda h_1} & (1-\kappa+2\lambda h_1)e^{\lambda h_1} & -2\lambda e^{-\lambda h_1} & (1-\kappa-2\lambda h_1)e^{-\lambda h_1} \\ -2i\lambda(\kappa-1) & i(\kappa^2-1) & -2i\lambda(\kappa-1) & i(1-\kappa^2) \\ -2\lambda & \kappa-1 & 2\lambda & \kappa-1 \\ -1 & 0 & -1 & 0 \\ -i & i\kappa/\lambda & i & i\kappa/\lambda \end{bmatrix} \quad (27a)$$

$$D'' = \begin{bmatrix} \Delta_1 & \Delta_2 & \Delta_3 & \Delta_4 \\ \Lambda_1 & \Lambda_2 & \Lambda_3 & \Lambda_4 \\ 1 & 1 & 1 & 1 \\ n_1 & n_2 & n_3 & n_4 \\ \Delta_1 e^{-m_1 h_2} & \Delta_2 e^{-m_2 h_2} & \Delta_3 e^{-m_3 h_2} & \Delta_4 e^{-m_4 h_2} \\ \Lambda_1 e^{-m_1 h_2} & \Lambda_2 e^{-m_2 h_2} & \Lambda_3 e^{-m_3 h_2} & \Lambda_4 e^{-m_4 h_2} \end{bmatrix} \quad (27b)$$

with

$$\Delta_k = -i\lambda(3-\kappa) + (1+\kappa)m_k n_k, \quad k = 1, \dots, 4 \quad (28a)$$

$$\Lambda_k = m_k - i\lambda n_k, \quad k = 1, \dots, 4 \quad (28b)$$